In-beam γ-ray spectroscopy of the neutron-rich platinum isotope ^{200}Pt toward the $N = 126$ shell gap

P. R. John,[1,2,*] J. J. Valiente-Dobón,[3] D. Mengoni,[1,2] V. Modamio,[3,†] S. Lunardi,[1,2] D. Bazzacco,[2] A. Gadea,[4] C. Wheldon,[5] T. R. Rodríguez,[6,7] T. Alexander,[8] G. de Angelis,[3] N. Ashwood,[5] M. Barr,[5] G. Benzoni,[9,10] B. Birkenbach,[11] P. G. Bizzeti,[12,13] A. M. Bizzeti-Sona,[12,13] S. Bottoni,[9,10,‡] M. Bowry,[8] A. Bracco,[9,10] F. Browne,[14] M. Bunce,[8] F. Camera,[9,10] L. Corradi,[3] F. C. L. Crespi,[9,10] B. Melon,[12,13] E. Farnea,[2] E. Fioretto,[3] A. Gottardo,[1,3,§] L. Grente,[15] H. Hess,[11] Tz. Kokalova,[5] W. Korten,[15] A. Kuşoğlu,[16,17] S. Lenzi,[1,2] S. Leoni,[9,10] J. Ljungvall,[18] R. Menegazzo,[1,2] C. Michelagnoli,[1,2,‖] T. Mijatović,[19] G. Montagnoli,[1,2] D. Montanari,[1,2,¶] D. R. Napoli,[3] Zs. Podolyák,[8] G. Pollarolo,[20,21] F. Recchia,[1,2] P. Reiter,[11] O. J. Roberts,[14,**] E. Şahin,[3,†] M.-D. Salsac,[15] F. Scarlassara,[1,2] M. Sferrazza,[22] P.-A. Söderström,[23,††] A. M. Stefanini,[3] S. Szilner,[18] C. A. Ur,[2,‡‡] A. Vogt,[11] and J. Walshe[5]

[1]*Dipartimento di Fisica e Astronomia, Università di Padova, I-35131 Padova, Italy*
[2]*Istituto Nazionale di Fisica Nucleare, Sezione di Padova, I-35131 Padova, Italy*
[3]*Istituto Nazionale di Fisica Nucleare, Laboratori Nazionali di Legnaro, I-35020 Legnaro, Italy*
[4]*Instituto de Física Corpuscular, CSIC-Universitat de València, E-46980 València, Spain*
[5]*School of Physics and Astronomy, University of Birmingham, Edgbaston, Birmingham B15 2TT, United Kingdom*
[6]*Institut für Kernphysik, Technische Universität Darmstadt, D-64289 Darmstadt, Germany*
[7]*Departamento de Física Teórica, Universidad Autónoma de Madrid, E-28049 Madrid, Spain*
[8]*Department of Physics, University of Surrey, GU2 7XH Guildford, United Kingdom*
[9]*Dipartimento di Fisica, Università di Milano, I-20133 Milano, Italy*
[10]*Istituto Nazionale di Fisica Nucleare, Sezione di Milano, I-20133 Milano, Italy*
[11]*Institut für Kernphysik, Universität zu Köln, D-50937 Köln, Germany*
[12]*Dipartimento di Fisica, Università di Firenze, I-50019 Sesto Fiorentino (Firenze), Italy*
[13]*Istituto Nazionale di Fisica Nucleare, Sezione di Firenze, I-50019 Sesto Fiorentino (Firenze), Italy*
[14]*School of Computing, Engineering and Mathematics, University of Brighton, Brighton BN2 4GJ, United Kingdom*
[15]*Institut de Recherche sur les lois Fondamentales de l'Univers IRFU, CEA/DSM, Centre CEA de Saclay, F-91191 Gif-sur-Yvette Cedex, France*
[16]*Department of Physics, Faculty of Science, Istanbul University, Vezneciler/Fatih, TR-34134 İstanbul, Turkey*
[17]*ELI-NP, Horia Hulubei National Institute of Physics and Nuclear Engineering, 077125 Magurele, Romania*
[18]*Centre de Spectrométrie Nucléaire et de Spectrométrie de Masse CSNSM, CNRS/IN2P3 and Université Paris-Sud, F-91405 Orsay Campus, France*
[19]*Institut Ruder Bošković, HR-10000 Zagreb, Croatia*
[20]*Dipartimento di Fisica Teorica, Università di Torino, I-10125 Torino, Italy*
[21]*Istituto Nazionale di Fisica Nucleare, Sezione di Torino, I-10125 Torino, Italy*
[22]*Département de Physique, Université libre de Bruxelles, B-1050 Bruxelles, Belgium*
[23]*Department of Physics and Astronomy, Uppsala University, SE-75120 Uppsala, Sweden*

(Received 28 March 2016; revised manuscript received 3 April 2017; published 22 June 2017)

The neutron-rich nucleus ^{200}Pt is investigated via in-beam γ-ray spectroscopy to study the shape evolution in the neutron-rich platinum isotopes towards the $N = 126$ shell closure. The two-neutron transfer reaction ^{198}Pt(^{82}Se, ^{80}Se)^{200}Pt is used to populate excited states of ^{200}Pt. The Advanced Gamma Ray Tracking Array (AGATA) demonstrator coupled with the PRISMA spectrometer detects γ rays coincident with the ^{80}Se recoils, the binary partner of ^{200}Pt. The binary partner method is applied to extract the γ-ray transitions and build the level scheme of ^{200}Pt. The level at 1884 keV reported by Yates *et al.* [S. W. Yates, E. M. Baum, E. A. Henry, L. G. Mann, N. Roy, A. Aprahamian, R. A. Meyer, and R. Estep, Phys. Rev. C **37**, 1889 (1988)] was confirmed to be at 1882.1 keV and assigned as the (6_1^+) state. An additional γ ray was found and it presumably deexcites the (8_1^+) state. The results are compared with state-of-the-art beyond mean-field calculations, performed for the even-even $^{190-204}$Pt isotopes, revealing that ^{200}Pt marks the transition from the γ-unstable behavior of lighter Pt nuclei towards a more spherical one when approaching the $N = 126$ shell closure.

DOI: 10.1103/PhysRevC.95.064321

*Present address: Institut für Kernphysik, Technische Universität Darmstadt, D-64289 Darmstadt, Germany; philipp.john@ikp.tu-darmstadt.de.

†Present address: Department of Physics, University of Oslo, P.O. Box 1048 Blindern, N-0316 Oslo, Norway.

‡Present address: Physics Division, Argonne National Laboratory, Argonne, Illinois 60439, USA.

§Present address: Centre de Spectrometrie Nucleaire et de Spectrometrie de Masse (CSNSM), CNRS/IN2P3 and Universite Paris-Sud, F-91405 Orsay Campus, France.

‖Present address: GANIL, CEA/DSM-CNRS/IN2P3, F-14076, Caen, France.

¶Present address: USIAS - Universite de Strasbourg, IPHC-CNRS, F-67037 Strasbourg Cedex 2, France.

Finite many-body systems such as molecules, many man-made nano-materials, and atomic nuclei exhibit nonspherical (deformed) ground states, representing a spontaneous symmetry breaking [1]. In atomic nuclei the deformed shape is due to the complex interplay between the residual nucleon-nucleon interactions driving towards deformation and the shell gaps that tend to restore the spherical shape. The study of the nuclear shape evolution along an isotopic chain opens a window on the underlying microscopic force and is an important testing ground for nuclear models [2].

One region of the nuclear chart, where oblate, prolate, γ-soft, and spherical shapes are observed and predicted is the tungsten-osmium-platinum region with $A \approx 190$. A prolate-to-oblate shape transition is predicted to appear when moving towards the $N = 126$ shell closure, where the spherical shape should be restored. For platinum and osmium isotopes such a shape transition occurs while passing through nuclei having a γ-soft potential. However, the path to sphericity is not yet fully expounded.

This region has been studied from a theoretical point of view via microscopic self-consistent mean-field approaches (Hartree-Fock-Bogoliubov, HFB) with a variety of interactions [3–10] revealing the importance of triaxial deformation. Another approach has been the interacting boson model, either purely phenomenological [10] or based on potential energy surfaces (PES) mapped to those obtained with HFB calculations with energy density functionals (EDF) [11,12]. State-of-the-art beyond-mean-field calculations based on energy density functionals have been successfully applied to reproduce the collective character of the ground-state bands in the osmium isotopic chain [13]. Such a theoretical framework, namely, the symmetry-conserving configuration-mixing (SCCM) method, includes simultaneous particle number and angular momentum projections and axial and nonaxial shape mixings [14–16] and provides information on both intrinsic deformations and the properties of excited levels in a natural manner.

The intrinsic deformation of the atomic nucleus is not a direct observable. To deduce the nuclear shape, in addition to the study of reduced electromagnetic transition probabilities, the energies of the excited levels can be used as a signature of the shape by comparison with theoretical models, such as the geometric models [17], which have different expectation values for ratios between the energies of excited states.

The study of excited states in the neutron-rich platinum isotopes approaching the $N = 126$ shell closure is experimentally challenging. While the less neutron-rich stable platinum isotopes were studied up to high spin via heavy-ion [18,19] and (α, xn) [20–26] fusion reactions, heavier platinum isotopes cannot be populated via fusion-evaporation reactions and stable beam-target combinations. Multinucleon-transfer reactions are complementary to fusion-evaporation reactions and have been used to study medium-to-high spin states in the ^{194,196,198}Pt isotopes [27–30]. Besides multinucleon transfer reactions, neutron-rich platinum isotopes were also studied via isomeric-decay spectroscopy after the fragmentation of a ^{208}Pb beam at relativistic energies. Due to the presence of isomeric states in ^{202}Pt [31,32] and in ^{204}Pt, ($N = 126$), the yrast band in these nuclei was established up to the (4_1^+) and 2_1^+ states, respectively.

Prior to this study, excited states of ^{200}Pt were studied via the ^{198}Pt$(t,p)^{200}$Pt reaction [33,34], via the β^- decay of ^{200}Ir [35], and via isomeric-decay spectroscopy after fragmentation of a ^{208}Pb at relativistic energies [31,32] due to the existence of two isomeric states.

The ratio between the energy of the first 4^+ and 2^+ states of ^{200}Pt indicates a change in structure from the predominately γ-soft lighter even-even platinum isotopes $^{194-198}$Pt. We have studied medium-spin excited states of ^{200}Pt via the ^{198}Pt(^{82}Se, ^{80}Se)^{200}Pt reaction and the binary partner method using the Advanced Gamma Tracking Array (AGATA) [36,37] demonstrator and the large acceptance magnetic spectrometer PRISMA [38–40]. The results are compared to SCCM calculations [15] using Gogny energy density functionals [41] that reproduce well the shape evolution of platinum isotopes when approaching the $N = 126$ shell closure.

I. EXPERIMENTAL SETUP AND DATA ANALYSIS

To produce neutron-rich isotopes around ^{198}Pt in excited states, a ^{82}Se beam was accelerated by the XTU Tandem-ALPI accelerator combination at the Laboratori Nazionali di Legnaro to an energy of 426 MeV. The beam impinged on a $2 - \mathrm{mg/cm^2}$-thick self-supporting ^{198}Pt target with an energy $\approx 11\%$ above the Coulomb barrier. Beamlike fragments were unambiguously identified in PRISMA by their atomic number, charge state, and mass. The time-of-flight range and the gas pressure of the ionization chamber of PRISMA were optimized for the study of neutron-rich nuclei around ^{198}Pt. The target was tilted by 5° to allow the targetlike and beamlike recoils to exit the target. The binary partner of the ion identified in PRISMA was stopped by the target chamber walls after a time-of-flight of around 10–15 ns.

Gamma rays in coincidence with an ion detected at the focal plane of PRISMA were measured by the AGATA demonstrator, which was placed at a distance of 15.5 cm from the target and opposing PRISMA with an angle of 180° to its optical axes. The setup of the experiment is drawn schematically in Fig. 1.

At the time of the experiment the AGATA demonstrator, from now on called AGATA, was in its full configuration of five triple clusters. Each cluster consists of three differently hexagonal tapered coaxial high-purity germanium detectors with 36 electrical-separated outer segments and a common inner core contact [42]. To reduce the counting rate in the first segments, a 600-μm-thick Sn absorber was installed in front of AGATA. In this configuration, AGATA had an angular coverage of 15% of 4π. The relative and absolute efficiency curve was derived using the ^{133}Ba, ^{152}Eu, and ^{60}Co standard

**Present address: University of York, Heslington, YO10 5DD York, United Kingdom.

††Present address: RIKEN Nishina Center, Wako, 351-0198 Saitama, Japan.

‡‡Present address: Extreme Light Infrastructure Nuclear Physics Facility, MG-6 Bucharest-Magurele, Romania.

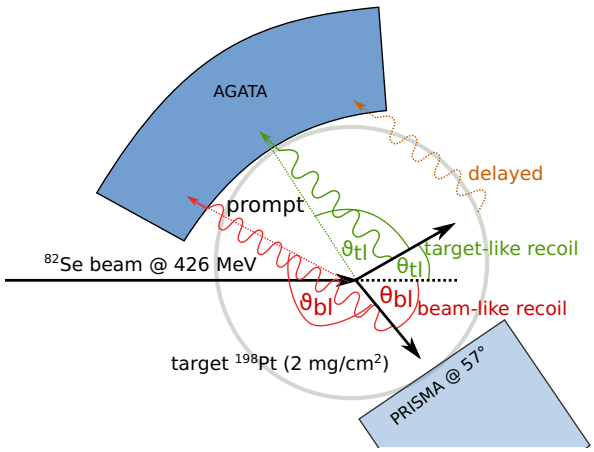

FIG. 1. Sketch of the experimental setup and the reaction kinematics of a typical event. The angles of the recoils are denoted by θ_{tl} and θ_{bl} and the angles for the Doppler correction are denoted by ϑ_{tl} and ϑ_{bl}. The dimensions are not to scale.

calibration sources. The efficiency after using the γ-ray tracking algorithm was $\approx 4\%$ at 1332.5 keV. The average rate per crystal was kept between 20 and 30 kHz during the whole experiment. The trigger was the coincidence of an ion arriving at the focal plane of PRISMA with at least one AGATA crystal (inner core). The signals were digitized and the energy and the wave form of the initial 1 μs was written to disk.

The position of each interaction in an AGATA segment is deduced by passing the digitized signals to a pulse shape analysis algorithm. The interaction positions together with their energies are used to reconstruct the γ rays by the Orsay forward tracking algorithm [43]. The emission time of the γ rays is deduced from the signal of the first interaction point, as identified by the tracking algorithm. The signals of the segments are aligned in time to the core signal. The time-dependent fully digitized signals are summed and the intersection between the baseline and the interpolated linear slope defines the time signal.

PRISMA provides the momentum vector of the beamlike recoil. This information is used together with the position of the first interaction inside AGATA for the Doppler correction for the γ rays emitted by the beamlike recoils. The momentum vector of the targetlike recoils is deduced event-by-event assuming a relativistic binary reaction without particle evaporation. However, the evaporation of neutrons is likely for excitation energies above the neutron-separation energy. Therefore, the deduced mass of the binary partner is just an upper limit. The energy loss of the reaction products in the target material is estimated for each event by employing the Northcliffe-Schilling approximation [44]. The full width at half maximum of the Doppler corrected γ-ray peaks is well below 1% for both beamlike and targetlike recoils.

Because the momentum and the angle of the beamlike recoils are measured simultaneously, the Q value of the reaction can be approximately reconstructed for each event. The reconstructed Q value has in this experiment an uncertainty that can reach up to 30 MeV due to the thickness of the target that is much higher than the neutron-separation energy of the neutron-rich platinum isotopes.

II. RESULTS

In the γ-ray spectrum gated on ^{80}Se and Doppler corrected for the binary partner, ^{200}Pt, γ-ray peaks from lighter platinum isotopes appear. To reduce the fraction of γ-ray peaks from ions produced by neutron evaporation in the γ-ray spectra, a condition on the low part of the reconstructed Q value is applied. This condition is the best compromise between statistics and the appearance of additional peaks due to neutron evaporation.

The two isomeric states, 7_1^- and (12_1^+), are populated in this reaction. Both have short half-lives of 17.0(5) and 13.9(10) ns [32], respectively. To enhance the true prompt events a condition on the initial-20-ns part of the prompt γ-ray peak is placed.

Figure 2(a) shows the Doppler-corrected γ-ray spectrum gated on ^{80}Se, the binary partner of ^{200}Pt. The most intense γ-ray peak in this spectrum is the $2_1^+ \rightarrow 0_{gs}^+$ (666 keV) transition of ^{80}Se. The Coulomb excitation of the ^{82}Se is reduced by placing a tight condition on the mass selection. However, peaks belonging to ^{82}Se cannot be completely suppressed, leading to a small γ-ray peak at 655 keV. The wrongly Doppler-corrected

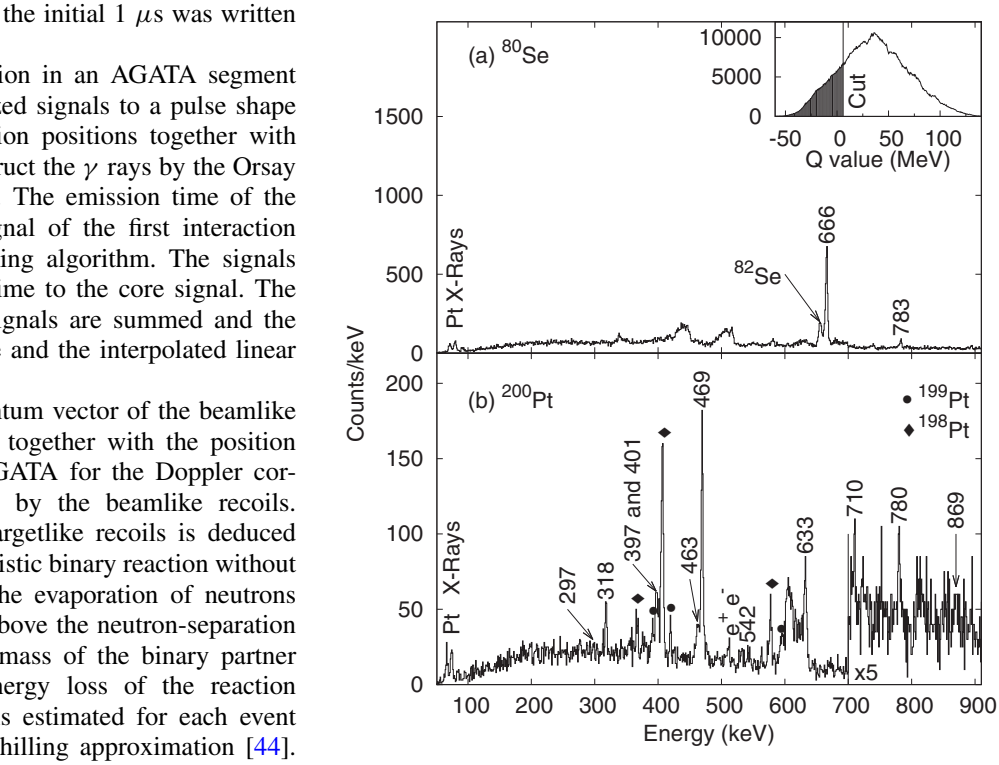

FIG. 2. The γ-ray spectra obtained after gating on the beamlike ^{80}Se recoils in PRISMA, at the low part of the reconstructed Q value and initial 20 ns of the prompt peak. (a) The spectrum is Doppler corrected for ^{80}Se. The strongest γ-ray transitions of ^{80}Se are labeled. (b) The spectrum is Doppler corrected for ^{200}Pt, the binary partner of ^{80}Se. Peaks labeled by energy are assigned to ^{200}Pt. The symbols mark γ-ray peaks belonging to lighter platinum isotopes.

γ-ray transitions belonging to the platinum isotopes appear as broad structures in the spectrum. In Fig. 2(b) the same spectrum is drawn, where the Doppler correction is performed for ^{200}Pt. The γ-ray peaks from ^{200}Pt and lighter platinum isotopes produced after the evaporation of neutrons are labeled by their energy and with different symbols, respectively. Due to the lifetime of the isomeric states, these γ rays are emitted mostly not at the target position. Hence, these peaks possess a tail in the Doppler-corrected γ-ray spectrum.

Besides the previously reported [31,32,34,35] ground-state band transitions at 469 and 633 keV, two γ-ray peaks at 780 and 869 keV appear in this spectrum that are assigned to the ground-state band of ^{200}Pt.

An energy level at 1884.0 keV was reported by Yates *et al.* [34] which deexcites to the 5_1^- and 4_1^+ states via γ rays of 317.4 and 780.8 keV having relative intensities of 29(9) and 36(5), respectively. This experiment confirms the γ-ray transition observed by Yates *et al.* [34] at 780 keV. The γ-ray peak that we observe in our spectra at 317.9 keV is a doublet composed of two transitions, the 317.4 keV deexciting the (6_1^+) level at 1882 keV (corresponding to the 1884-keV level of Ref. [34]) to the 5_1^- level at 1565 keV and the transition at 318.4 keV feeding the 7_1^- isomeric state [31,32]. The relative intensities of the 317.4- and 780.8-keV transitions reported in Ref. [34] have been used to extract the intensity of the 317.4-keV transition in the doublet and, as a consequence, the one of the 318.4-keV transition.

To verify this assignment a γ-γ-coincidence analysis is performed with a γ-γ matrix produced using the same conditions as for the creation of the spectrum in Fig. 2: the γ-γ matrix was constructed placing a gate on the identified ^{80}Se isotopes, on the low reconstructed Q value and on the early part of the prompt peak with a 20-ns-wide gate.

The results are shown in Fig. 3. The $2_1^+ \rightarrow 0_{gs}^+$ and $4_1^+ \rightarrow 2_1^+$ transitions are in mutual coincidence with each other and the 780- and 869-keV γ-ray peaks. A coincidence between the 780- and 869-keV γ-ray peaks is not observed. This is expected due to statistical consideration and the efficiency of AGATA: due to the statistics, the absence of a coincidence between the 869- and 780-keV transitions can be estimated with a binomial distribution. The content of the 869-keV γ-ray peak is 12 counts in the spectrum. Considering the absolute efficiency at the energy of the $(6_1^+) \rightarrow (4_1^+)$ transition, the probability of having 0 counts in coincidence is $51.3^{+23.5}_{-43.3}$%. The same analysis yields for the observed coincidences between the 869 keV γ-ray peak and the 469- and 633-keV transitions $48.9^{+45.3}_{-23.5}$% and $36.0^{+0.2}_{-30.3}$%, respectively.

Yates *et al.* [34] populated excited states in ^{200}Pt via the (t,p) reaction and reported the observation of a 780.8-keV γ-ray feeding the 4_1^+ state without any spin and parity assignment. In different experiments, the excitation of the 6_1^+ level in the (t,p) reaction was observed for the platinum isotopes ^{196}Pt and ^{198}Pt [33,45]. Therefore, from systematics the assignment as the (6_1^+) state is compatible with the previous observation of this level.

In addition, Yates *et al.* [34] reported a weak decay branch from the second 2^+ to the ground state with an energy of 867 keV, which is within the uncertainty of the 869-keV transition. This transition does not correspond to the observed γ-ray peak, because clear coincidences with the $4_1^+ \rightarrow 2_1^+$ and $2_1^+ \rightarrow 0_{gs}^+$ transitions are observed that are in anticoincidence with a $2_2^+ \rightarrow 0_{gs}^+$ transition.

The results are summarized in Table I and the proposed level scheme is shown in Fig. 4 in which the decay sequence of the isomeric states, based on Refs. [31,34], is shown for completeness.

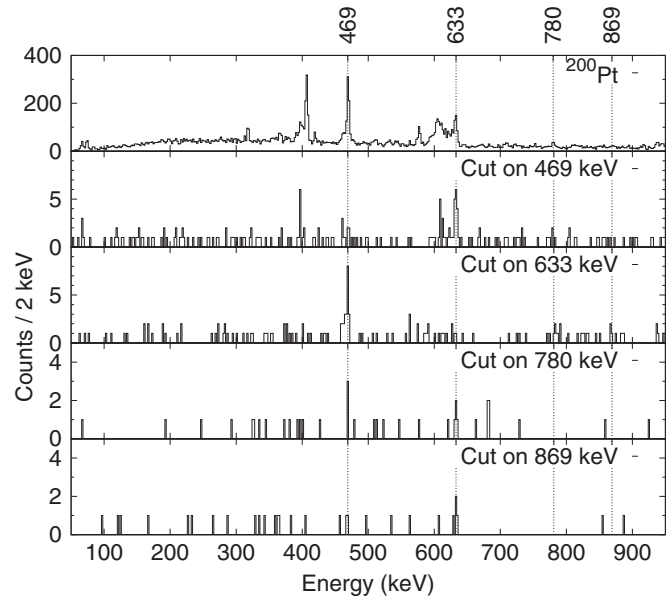

FIG. 3. The γ-ray spectrum obtained for ^{200}Pt after gating on the beamlike ^{80}Se recoils having a low reconstructed Q value and with a gate on the γ rays at 470, 633, 780, and 869 keV.

TABLE I. Energies (E_γ) and relative intensities (I_γ) of the observed γ-ray transitions for ^{200}Pt. The intensities are given with a condition on the low part of the reconstructed Q value [spectrum, Fig. 2(b)]. The spin assignment of the transitions and the energy of the level [$E(J_i)$] are also given. See text for details.

E_γ (keV)	I_γ	$J_i^\pi \rightarrow J_f^\pi$	$E(J_i)$ (keV)
297.4(10)	3(3)	$5_1^- \rightarrow 4_2^+$	1564.5
317.4(10)	8(4)[a]	$(6_1^+) \rightarrow 5_1^-$	1882.1
318.4(10)	9(5)[a]		
397.0(10)	24(6)	$2_2^+ \rightarrow 2_1^+$	866.6
400.6(10)	15(5)	$4_2^+ \rightarrow 2_2^+$	1267.2
462.7(10)	19(4)	$5_1^- \rightarrow 4_1^+$	1564.5
469.4(10)	100(6)	$2_1^+ \rightarrow 0_{gs}^+$	469.4
541.8(10)	4(3)		
633.2(10)	46(5)	$4_1^+ \rightarrow 2_1^+$	1101.7
709.6(10)	6(4)		
780.4(20)	9(4)	$(6_1^+) \rightarrow 4_1^+$	1882.1
869(3)	2(2)	$(8_1^+) \rightarrow (6_1^+)$	2751

[a]Doublet intensity balance based on Ref. [34].

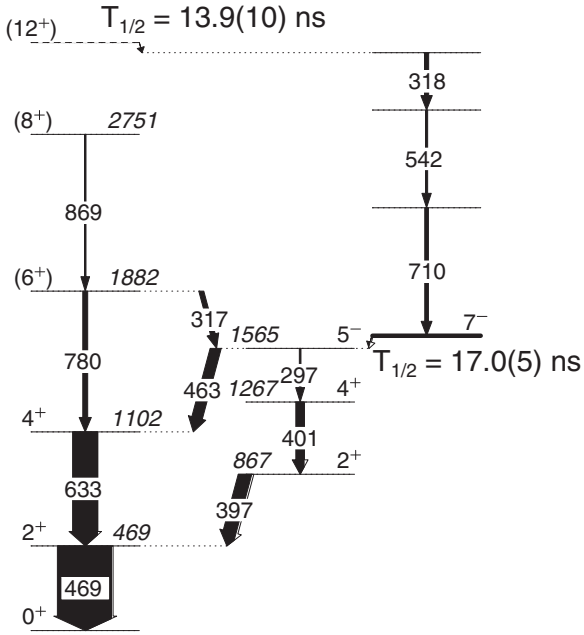

FIG. 4. Level scheme of ^{200}Pt deduced from the present data. The placement of the transitions deexciting the isomeric states is based on Ref. [31]. The half-lives of the isomeric states are taken from Ref. [32].

III. DISCUSSION

To better understand the collective character and the shape evolution in this region, SCCM calculations based on Gogny D1S energy density functionals have been performed for $^{190-204}$Pt isotopes. Nuclear states are defined in this method as linear combinations of particle-number- and angular-momentum-projected HFB wave functions with different quadrupole shapes (axial and nonaxial). Hence, the coefficients of such configuration mixings are obtained self-consistently by using the generator coordinate method [46]. On the other hand, the intrinsic HFB wave functions are found through a variation after particle number projection method (PN-VAP) [47] imposing constraints on the quadrupole deformation (β_2,γ). Additionally, these intrinsic HFB wave functions do not break either reflection or time-reversal symmetries. Therefore, only positive-parity states can be described and a systematic stretching of the theoretical spectra with respect to the experimental data is expected [48]. A detailed description of the present SCCM method can be found in Ref. [15].

As a first step, one can analyze qualitatively the shape of a given nucleus by studying its PES, i.e., the energy as a function of the intrinsic deformations. In Fig. 5 the PESs in the (β_2,γ) plane for $^{190-204}$Pt isotopes are presented, calculated with a PN-VAP method. Here, one observes only one minimum in each PES, which evolves rather smoothly from a triaxial deformed shape—$(\beta_2,\gamma) \approx (0.15,40^\circ)$—in ^{190}Pt, to an axial oblate deformation—$(\beta_2,\gamma) \approx (0.10,60^\circ)$—in ^{196}Pt, to a much less deformed oblate—$(\beta_2,\gamma) \approx (0.05,60^\circ)$—in ^{200}Pt when approaching the $N = 126$ spherical shell closure. Here (^{204}Pt), a spherical magic nucleus is found. A similar behavior of the PESs has been already obtained with other EDFs [6,10,11,49].

A more quantitative analysis of the collective character of the isotopic chain is the study of the ratio of the excitation energies of the ground-state band with respect to the value of the excitation energy of the first 2^+ state. In Fig. 6 the theoretical results obtained with the SCCM method described above and the available experimental data are represented for $^{190-204}$Pt nuclei. In addition, the predictions for the axial rotor, vibrator, and γ-unstable/triaxial rotor geometrical models are plotted. The experimental data are taken from Refs. [35,50–52] and this work for ^{196,198,200}Pt. The latter limit is reproduced almost perfectly with the microscopic calculations in the

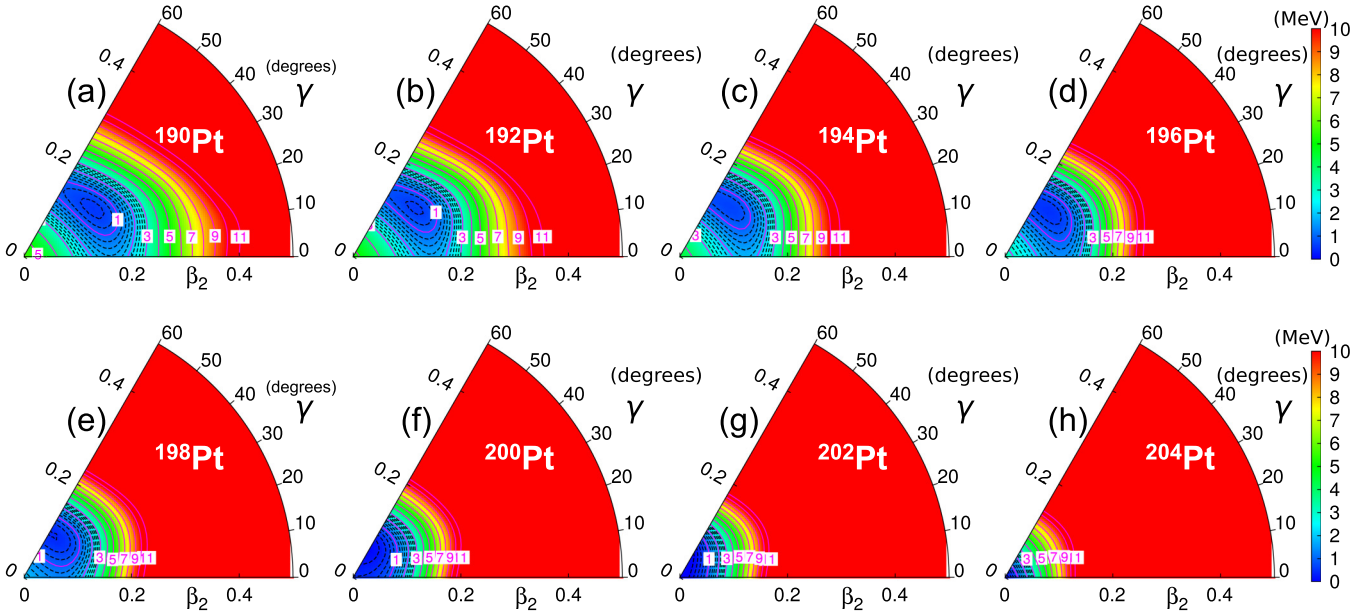

FIG. 5. Particle-number-projected potential energy surfaces in the triaxial plane for $^{190-204}$Pt isotopes calculated with the Gogny D1S interaction. Solid and dashed contour lines are separated by 1.0 and 0.2 MeV, respectively.

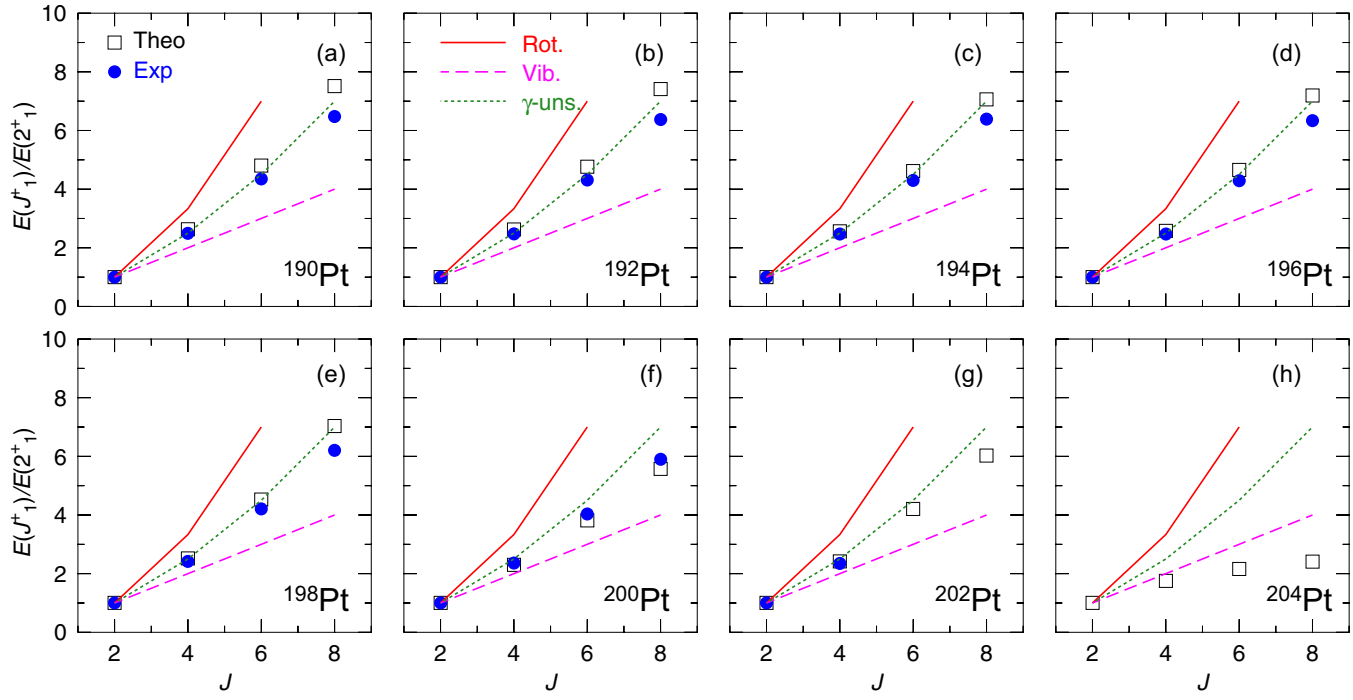

FIG. 6. Yrast band excitation energies, normalized to the corresponding 2_1^+ energies, for $^{190-204}$Pt isotopes. Blue dots and black boxes are the experimental points and theoretical beyond-mean-field predictions, respectively. Theoretical limits for axial rotor (red continuous line), vibrator (magenta dashed line), and γ-unstable/triaxial rotor (green dotted line) geometrical models are also given. The experimental data are taken from Ref. [35,50–52] and this work for ^{196,198,200}Pt.

isotopes $^{194-198}$Pt, while for $^{190-192}$Pt and ^{200}Pt tiny deviations from this limit towards a more axial rotational character and a more vibrational character, respectively, are observed. The states (6^+) and (8^+) that have been associated with the γ-ray peaks at 780 and 869 keV in ^{200}Pt agree well with the SCCM calculations, supporting the spin and parity assignment. For the semimagic isotope ^{204}Pt, the predictions lie even below the vibrational limit, although for these nuclei explicit quasiparticle excitations not included in the present framework could play a major role in describing low-lying excited states.

Summarizing, the even-even $^{190-200}$Pt isotopes exhibit a γ-soft potential energy surface and the excited states lie close to the γ-unstable/triaxial rotor geometrical model. The deformation decreases approaching the $N = 126$ subshell closure and the nucleus ^{200}Pt marks the transition towards a more spherical behavior. Hence, for ^{204}Pt, the potential energy surface is purely spherical and the excited states, as stated before, go even below the vibrational limit. For the ^{202}Pt isotope the potential energy surface follows the general trend where the minimum tends towards sphericity. However, the ratio shown in Fig. 6(g) shows a slightly more γ-soft behavior than in ^{200}Pt, changing the trend towards the spherical ^{204}Pt. The reason for this anomaly has to be found in the subtle evolution of the shape of the excited states individually. While for ^{200}Pt the excited states evolve towards the triaxial degree of freedom with an almost constant β_2 value of 0.07, for ^{202}Pt the excited states remain axial oblate deformed with a small increase in deformation as a function of the angular momentum from $\beta_2 = 0.05$ (almost spherical) for the 0_1^+ state to $\beta_2 = 0.10$ for the 8_1^+ state. Therefore, the observed increased in the $E(J_1^+)/E(2_1^+)$ ratio in ^{202}Pt reflects the slight increase in the deformation of the excited states and not the return towards the γ-unstable/triaxial rotor. In fact, this theoretical limit only has a well-defined meaning when the deformation remains constant for all the states, which is not the case for ^{202}Pt.

The comparison with the experimental data is rather good although a slightly less rotational character than the theoretical predictions is shown in ^{190,198}Pt. Nevertheless, the evolution from triaxial collective character towards a vibrational spectrum when approaching the $N = 126$ shell gap is well reproduced.

IV. SUMMARY

Medium-high ground-state band states in ^{200}Pt have been studied via in-beam γ-ray spectroscopy using the AGATA demonstrator coupled with the large acceptance PRISMA magnetic spectrometer employing the ^{198}Pt(^{82}Se, ^{80}Se)^{200}Pt reaction. Two additional states were assigned to the ground-state band extending the yrast band up to the (8_1^+) level. The nuclear shape evolution of the even-even $^{190-204}$Pt isotopes was studied via state-of-the art SCCM calculations. The theoretical predictions agree well with the experimental data. In particular the ground-state band of ^{200}Pt is well reproduced, revealing its nature as a transitional nucleus between the lighter γ-unstable platinum isotopes and the presumably spherical $N = 126$ platinum isotope ^{204}Pt. Additional experimental studies including the measurement of higher-lying excited states in ^{202}Pt and ^{204}Pt and measurements of the quadrupole

moment of the neutron-rich platinum isotopes in the vicinity of the $N = 126$ shell closure will help us to further understand the shape evolution in the neutron-rich platinum isotopes.

ACKNOWLEDGMENTS

The authors want to thank the partial funding of this project by BMBF Projects No. 06DA7047I and No. 05P12PKFNE; the Ministerio de Economía y Competitividad, Spain, under Programa Ramón y Cajal 2012, Grants No. AIC-D-2011-0746, No. FPA2011-29854, No. FPA-2011-29854-C04-01, and No. FIS2014-53434-P; the Spanish Consolider-Ingenio 2010 Programme CPAN (Grant No. CSD2007-00042); the UK Science and Technology Facilities Council (STFC); the Generalitat Valenciana, Spain, under Grant No. PROMETEO/2010/101; the Scientific Research Projects Coordination Unit of Istanbul University under Project No. 15539; a Daphne Jackson Fellowship; the IAP program P6/23 Belgian State-BSP; the Polish Ministry of Science and Higher Education (Grant No. DPN/N190/AGATA/2009); and by the European Union Seventh Framework Programme FP7/2007-2013 under Grant Agreement No. 262010.

[1] R. Broglia, Surf. Sci. **500**, 759 (2002).
[2] K. Heyde and J. L. Wood, Rev. Mod. Phys. **83**, 1467 (2011).
[3] R. Bengtsson *et al.*, Phys. Lett. B **183**, 1 (1987).
[4] M. M. Sharma and P. Ring, Phys. Rev. C **46**, 1715 (1992).
[5] R. Fossion, D. Bonatsos, and G. A. Lalazissis, Phys. Rev. C **73**, 044310 (2006).
[6] T. Nikšić, P. Ring, D. Vretenar, Y. Tian, and Z.-y. Ma, Phys. Rev. C **81**, 054318 (2010).
[7] L. M. Robledo *et al.*, J. Phys. G **36**, 115104 (2009).
[8] A. Ansari, Phys. Rev. C **33**, 321 (1986).
[9] P. Sarriguren, R. Rodríguez-Guzmán, and L. M. Robledo, Phys. Rev. C **77**, 064322 (2008).
[10] J. E. García-Ramos, K. Heyde, L. M. Robledo, and R. Rodríguez-Guzmán, Phys. Rev. C **89**, 034313 (2014).
[11] K. Nomura, T. Otsuka, R. Rodríguez-Guzmán, L. M. Robledo, and P. Sarriguren, Phys. Rev. C **83**, 014309 (2011).
[12] K. Nomura, T. Otsuka, R. Rodríguez-Guzmán, L. M. Robledo, and P. Sarriguren, Phys. Rev. C **84**, 054316 (2011).
[13] P. R. John, V. Modamio, J. J. Valiente-Dobón, D. Mengoni, S. Lunardi, T. Rodríguez, D. Bazzacco, A. Gadea, C. Wheldon, T. Alexander *et al.*, Phys. Rev. C **90**, 021301 (2014).
[14] M. Bender and P.-H. Heenen, Phys. Rev. C **78**, 024309 (2008).
[15] T. R. Rodríguez and J. L. Egido, Phys. Rev. C **81**, 064323 (2010).
[16] J. M. Yao, J. Meng, P. Ring, and D. Vretenar, Phys. Rev. C **81**, 044311 (2010).
[17] J. Zhang *et al.*, Phys. Lett. B **407**, 201 (1997).
[18] G. Li, M. Liu, X. Zhou, Y. Zhang, Y. Liu, N. Zhang, W. Hua, Y. Zheng, Y. Fang, S. Guo *et al.*, Phys. Rev. C **89**, 054303 (2014).
[19] Y. Oktem, D. Balabanski, B. Akkus, C. Beausang, M. Bostan, R. Cakirli, R. Casten, M. Danchev, M. Djongolov, M. Erduran *et al.*, Phys. Rev. C **76**, 044315 (2007).
[20] L. Funke, P. Kemnitz, G. Winter, S. Hjorth, A. Johnson, and T. Lindblad, Phys. Lett. B **55**, 436 (1975).
[21] S. Hjorth, A. Johnson, T. Lindblad, L. Funke, P. Kemnitz, and G. Winter, Nucl. Phys. A **262**, 328 (1976).
[22] S. Yates, J. Cunnane, R. Hochel, and P. Daly, Nucl. Phys. A **222**, 301 (1974).
[23] A. Levon, Y. V. Nosenko, V. Onischuk, A. Schevchuk, and A. Stuchbery, Nucl. Phys. A **764**, 24 (2006).
[24] J. Cunnane, M. Piiparinen, P. Daly, C. Dors, T. Khoo, and F. Bernthal, Phys. Rev. C **13**, 2197 (1976).
[25] I. Kovgar, A. Levon, R. Poznyak, and O. Sevastyuk, Phys. At. Nucl. **64**, 843 (2001).
[26] M. Piiparinen, J. Cunnane, P. Daly, C. Dors, F. Bernthal, and T. Khoo, Phys. Rev. Lett. **34**, 1110 (1975).
[27] S. Wahid, S. Tandel, P. Chowdhury, R. Janssens, M. Carpenter, T. Khoo, F. Kondev, T. Lauritsen, C. Lister, D. Seweryniak *et al.*, Phys. Rev. C **92**, 054323 (2015).
[28] G. A. Jones, Zs. Podolyák, N. Schunck, P. M. Walker, G. De Angelis, Y. H. Zhang, M. Axiotis, D. Bazzacco, P. G. Bizzeti, F. Brandolini *et al.*, Acta Phys. Pol., B **36**, 1323 (2005).
[29] S. Tandel, S. Wahid, P. Chowdhury, R. Janssens, M. Carpenter, T. Khoo, F. Kondev, T. Lauritsen, C. Lister, D. Seweryniak *et al.*, Phys. Lett. B **750**, 225 (2015).
[30] J. J. Valiente-Dobón *et al.*, Phys. Rev. C **69**, 024316 (2004).
[31] M. Caamaño *et al.*, Eur. Phys. J. A **23**, 201 (2005).
[32] S. J. Steer *et al.*, Phys. Rev. C **84**, 044313 (2011).
[33] J. A. Cizewski, E. R. Flynn, R. E. Brown, D. L. Hanson, S. D. Orbesen, and J. W. Sunier, Phys. Rev. C **23**, 1453 (1981).
[34] S. W. Yates, E. M. Baum, E. A. Henry, L. G. Mann, N. Roy, A. Aprahamian, R. A. Meyer, and R. Estep, Phys. Rev. C **37**, 1889 (1988).
[35] A. Morales, J. Benlliure, M. Gorska, H. Grawe, S. Verma, P. Regan, Z. Podolyak, S. Pietri, R. Kumar, E. Casarejos *et al.*, Phys. Rev. C **88**, 014319 (2013).
[36] A. Gadea *et al.*, Nucl. Instrum. Methods Phys. Res., Sect. A **654**, 88 (2011).
[37] S. Akkoyun *et al.*, Nucl. Instrum. Methods Phys. Res., Sect. A **668**, 26 (2012).
[38] A. M. Stefanini *et al.*, Nucl. Phys. A **701**, 217 (2002).
[39] S. Szilner, C. A. Ur, L. Corradi, N. Mărginean, G. Pollarolo, A. M. Stefanini, S. Beghini, B. R. Behera, E. Fioretto, A. Gadea *et al.*, Phys. Rev. C **76**, 024604 (2007).
[40] D. Montanari *et al.*, Eur. Phys. J. A **47**, 1 (2011).
[41] J. F. Berger *et al.*, Nucl. Phys. A **428**, 23 (1984).
[42] A. Wiens, H. Hess, B. Birkenbach, B. Bruyneel, J. Eberth, D. Lersch, G. Pascovici, P. Reiter, H.-G. Thomas, A. Collaboration *et al.*, Nucl. Instrum. Methods Phys. Res., Sect. A **618**, 223 (2010).
[43] A. Lopez-Martens *et al.*, Nucl. Instrum. Methods Phys. Res., Sect. A **533**, 454 (2004).
[44] L. C. Northcliffe and R. F. Schilling, At. Data Nucl. Data Tables **7**, 233 (1970).
[45] J. Cizewski, E. Flynn, R. E. Brown, and J. Sunier, Phys. Lett. B **88**, 207 (1979).

[46] P. Ring and P. Schuck, *The Nuclear Many-Body Problem* (Springer, New York, 2004).
[47] M. Anguiano, J. L. Egido, and L. M. Robledo, Nucl. Phys. A **696**, 467 (2001).
[48] M. Borrajo, T. R. Rodríguez, and J. L. Egido, Phys. Lett. B **746**, 341 (2015).
[49] R. Rodríguez-Guzmán, P. Sarriguren, L. M. Robledo, and J. E. García-Ramos, Phys. Rev. C **81**, 024310 (2010).
[50] B. Singh, Nucl. Data Sheets **99**, 275 (2003).
[51] C. M. Baglin, Nucl. Data Sheets **113**, 1871 (2012).
[52] B. Singh, Nucl. Data Sheets **107**, 1531 (2006).